The complex variable reproducing kernel particle method for two-dimensional elastodynamics*

Chen Li(陈 丽)[a] and Cheng Yu-Min(程玉民)[b]†

[a] *Department of Engineering Mechanics, Chang'an University, Xi'an* 710064, *China*
[b] *Shanghai Institute of Applied Mathematics and Mechanics, Shanghai University, Shanghai* 200072, *China*

(Received 28 January 2010; revised manuscript received 24 February 2010)

On the basis of the reproducing kernel particle method (RKPM), a new meshless method, which is called the complex variable reproducing kernel particle method (CVRKPM), for two-dimensional elastodynamics is presented in this paper. The advantages of the CVRKPM are that the correction function of a two-dimensional problem is formed with one-dimensional basis function when the shape function is obtained. The Galerkin weak form is employed to obtain the discretised system equations, and implicit time integration method, which is the Newmark method, is used for time history analysis. And the penalty method is employed to apply the essential boundary conditions. Then the corresponding formulae of the CVRKPM for two-dimensional elastodynamics are obtained. Three numerical examples of two-dimensional elastodynamics are presented, and the CVRKPM results are compared with the ones of the RKPM and analytical solutions. It is evident that the numerical results of the CVRKPM are in excellent agreement with the analytical solution, and that the CVRKPM has greater precision than the RKPM.

Keywords: meshless method, reproducing kernel particle method, complex variable reproducing kernel particle method, elastodynamics

PACC: 0260, 0270, 4630C

1. Introduction

Transient analysis for engineering structures subjected to dynamic loads is very important. The transient elastodynamics problems are classically described by a linear or nonlinear partial differential equation associated with boundary conditions and initial conditions. It is usually very difficult to obtain the solutions of these transient elastodynamic problems analytically. Therefore, for many decades, researchers have put in considerable efforts to develop efficient numerical methods to solve these problems. The finite element method (FEM) and the boundary element method (BEM) are undoubtedly the dominant methods for modelling transient elastodynamic problems at present.[1] The FEM and the BEM are the numerical method based on mesh, so it is necessary to deal with extremely large deformations of mesh with the re-meshing technique. Researchers are always looking for more efficient computational methods that can reduce the re-meshing process or avoid complicated mathematical manipulation. The meshless method is an interesting numerical technique that can solve many engineering problems not suitable for conventional numerical methods with a minimum of meshing or no meshing at all.[2,3]

Many meshless methods have been developed, such as smoothed particle hydrodynamics (SPH),[4] the diffuse element method (DEM),[5] element-free Galerkin (EFG) method,[6] reproducing kernel particle method (RKPM),[7] finite point method (FPM),[8] meshless local Petrov–Galerkin (MLPG) method,[9] meshless point collocation method (PCM),[10] wavelet particle method (WPM),[11] radial basis functions (RBFs),[12] meshless finite element method (MFEM),[13] complex variable meshless method,[14−16] and the meshless boundary integral equation methods.[17−27]

In recent years, some meshless methods have been gradually applied to linear elastodynamic problems. Belytschko *et al.* have used the EFG method to solve dynamic fracture problems.[28] Liu *et al.*[29] proposed the RKPM for structural dynamics analysis. Han and Atluri[30] presented the MLPG approach for three-dimensional elastodynamics. Liu *et al.*[31] presented a simple and less-costly MLPG method for the dynamic fracture problem. The MLPG method was ap-

*Project supported by the National Natural Science Foundation of China (Grant No. 10871124), and the Innovation Program of Shanghai Municipal Education Commission, China (Grant No. 09ZZ99).
†Corresponding author. E-mail: ymcheng@shu.edu.cn cc ymcheng@sh163.net
© 2010 Chinese Physical Society and IOP Publishing Ltd

plied to analyse free and forced vibration of solids by Gu and Lin[32] Bueche *et al.*[33] applied the natural element method (NEM) to obtain the solution of two-dimensional (2D) linear elastodynamics. Li and Cheng presented the meshless manifold method to analyse transient deformation and dynamic fracture problems.[34,35] Cheng and Peng[22] and Liew *et al.*[23] presented a direct meshless boundary integral equation method, called boundary element-free method (BEFM), to solve 2D linear elastodynamic problems. Sladek *et al.*,[36] Sellountos and Polyzos[37] applied the meshless local boundary integral equation (LBIE) method to elastodynamic problems. Lam group[38] applied Local Kriging (LoKriging) method to structural dynamic analysis. Liew and Cheng[39] presented the complex variable boundary element-free method (CVBEFM) to solve 2D elastodynamic problems.

The SPH method, which is based on the kernel estimate introduced by Monaghan, is the earliest meshless method.[4,40] To overcome the loss of accuracy of the SPH in a finite domain, Liu *et al.* proposed the RKPM to improve the performance of the SPH by introducing a correction function to the kernel function of integral transformation in the SPH method.[7] By imposing the reproducing conditions, the resulting modified kernel function reproduces polynomials exactly to a specific order and fulfills the completeness requirement. The RKPM not only shares the common features of all meshless methods but also has some unique features, such as time or space localisation, hp-like adaptivity as well as multiresolution analysis.[41] All these make the RKPM a novel approach for structural dynamics,[29,42–45] large deformation problems,[46,47] and fluid mechanics.[48]

Though the RKPM has lots of advantages over other conventional numerical methods, the meshless method formed with it has great computational cost because of a great number of nodes selected in the domain of a problem, and the shape functions that must be obtained at every node. Then the complex variables reproducing kernel particle method (CVRKPM) was presented by the authors of this paper, and the 2D elasticity problems and transient heat conduction problems were solved with the CVRKPM.[49,50] The CVRKPM is an approximation of a vector function, and the correction function of a 2D problem is formed with 1D basis function when the shape function is obtained with the CVRKPM. Some examples given in Refs. [49] and [50] demonstrated that the CVRKPM has greater precision and computational efficiency than the RKPM.

In this paper, the CVRKPM for the 2D elastodynamics is presented. The Galerkin weak form is employed to obtain the discretised system equations, and the implicit time integration method, which is the Newmark method, is used for time history analysis. The penalty method is employed to apply the essential boundary conditions. Then the corresponding formulae of the CVRKPM for 2D elastodynamics are obtained. Three numerical examples of 2D elastodynamics are presented, and the CVRKPM results are compared with the RKPM ones and analytical solutions. It is evident that the numerical results of the CVRKPM are in excellent agreement with the analytical solution, and that the CVRKPM has greater precision than the RKPM.

2. Complex variable reproducing kernel particle method

In this section, the formulae of the shape function of the CVRKPM are discussed in detail.

The CVRKPM is an approximation to a vector function, but the RKPM is an approximation to a scalar function.

2.1. Complex variable reproducing kernel approximation

Similar to the RKPM, the CVRKPM is also a class of operators that reproduce the function itself through the integration over the entire domain. The reproducing kernel approximation $\bar{u}^h(z)$ of a complex function $\bar{u}(z) = u_1(z) + \mathrm{i}u_2(z)$ is given by

$$\bar{u}^h(z) = u_1^h(z) + \mathrm{i}\, u_2^h(z) = \int_\Omega \bar{u}(z') \cdot \bar{w}_\mathrm{h}(z - z')\mathrm{d}z', \quad (z = x_1 + \mathrm{i}\, x_2 \in \Omega), \tag{1}$$

where $\bar{w}_\mathrm{h}(z - z')$ is a corrected reproducing kernel function

$$\bar{w}_\mathrm{h}(z - z') = C(z; z - z') \cdot w_\mathrm{h}(z - z'); \tag{2}$$

$w_\mathrm{h}(z - z')$ is the kernel function which has a compact support domain, and the cubic spline function is chosen as the weight function in this paper; $C(z; z - z')$ is the correction function and is also expressed as a linear combination of polynomial basis functions, i.e.

$$C(z; z - z') = \sum_{i=0}^{m} p_i(z - z') \cdot b_i(z) = \boldsymbol{p}^\mathrm{T}(z - z')\boldsymbol{b}(z). \tag{3}$$

Here m is the highest order of polynomial basis functions, $p_i(z-z')$ are the basis functions, and $b_i(z)$ are the corresponding coefficients.

In general, for 2D problems, the basis functions can be chosen as

• Linear basis:

$$\boldsymbol{p}^{\mathrm{T}} = (1, z-z'), \quad m=1; \tag{4}$$

• Quadratic basis:

$$\boldsymbol{p}^{\mathrm{T}} = \left(1, z-z', (z-z')^2\right), \quad m=2. \tag{5}$$

2.2. Complex variable particle approximation

Suppose that the domain Ω is discretised by a set of nodes $(z_1, z_2, \ldots, z_n)$, where z_I is the location of node I, and n is the total number of nodes. By the use of a simple trapezoidal rule, Eq. (1) is approximated by the following summation for all the nodes in the domain Ω:

$$\begin{aligned}\bar{u}^h(z) &= \sum_{I=1}^{n} \bar{u}(z_I)\cdot \bar{w}_{\mathrm{h}}(z-z_I)\cdot \Delta V_I \\ &= \sum_{I=1}^{n} C(z; z-z_I)\cdot w_{\mathrm{h}}(z-z_I) \\ &\quad \cdot \Delta V_I \cdot \bar{u}(z_I),\end{aligned} \tag{6}$$

where ΔV_I is the volume of node z_I and represents the integration weight, and

$$\bar{u}(z_I) = u_1(z_I) + \mathrm{i}\, u_2(z_I). \tag{7}$$

Equation (6) can be written as

$$\bar{u}^h(z) = \boldsymbol{C}(z)\boldsymbol{W}(z)\boldsymbol{V}\cdot\bar{\boldsymbol{u}}, \tag{8}$$

where

$$\bar{\boldsymbol{u}} = (\bar{u}(z_1), \bar{u}(z_2), \ldots, \bar{u}(z_n))^{\mathrm{T}} = \boldsymbol{Q}\boldsymbol{u}; \tag{9}$$

$$\begin{aligned}\boldsymbol{u} = (&u_1(z_1), u_2(z_1), u_1(z_2), u_2(z_2), \ldots, \\ &u_1(z_n), u_2(z_n))^{\mathrm{T}},\end{aligned} \tag{10}$$

$$\boldsymbol{Q} = \begin{bmatrix} 1 & i & 0 & 0 & 0 & 0 & \ldots & 0 & 0 \\ 0 & 0 & 1 & i & 0 & 0 & \ldots & 0 & 0 \\ 0 & 0 & 0 & 0 & 1 & i & \ldots & 0 & 0 \\ \vdots & \vdots & \vdots & \vdots & \vdots & \vdots & \ddots & \vdots & \vdots \\ 0 & 0 & 0 & 0 & 0 & 0 & \ldots & 1 & i \end{bmatrix}_{n\times 2n}, \tag{11}$$

$$\boldsymbol{W}(z) = \begin{bmatrix} w_{\mathrm{h}}(z-z_1) & 0 & \ldots & 0 \\ 0 & w_{\mathrm{h}}(z-z_2) & \ldots & 0 \\ \vdots & \vdots & \ddots & \vdots \\ 0 & 0 & \ldots & w_{\mathrm{h}}(z-z_n) \end{bmatrix}, \tag{12}$$

$$\boldsymbol{V} = \begin{bmatrix} \Delta V_1 & 0 & \ldots & 0 \\ 0 & \Delta V_2 & \ldots & 0 \\ \vdots & \vdots & \ddots & \vdots \\ 0 & 0 & \ldots & \Delta V_n \end{bmatrix}. \tag{13}$$

Let

$$C_I(z) = C(z; z-z_I) = \boldsymbol{p}^{\mathrm{T}}(z-z_I)\boldsymbol{b}(z), \tag{14}$$

then

$$\boldsymbol{C}(z) = (C_1(z), C_2(z), \ldots, C_n(z)) = \boldsymbol{b}^{\mathrm{T}}(z)\boldsymbol{P}, \tag{15}$$

where

$$\boldsymbol{P} = \begin{bmatrix} p_0(z-z_1) & p_0(z-z_2) & \ldots & p_0(z-z_n) \\ p_1(z-z_1) & p_1(z-z_2) & \ldots & p_1(z-z_n) \\ \vdots & \vdots & \ddots & \vdots \\ p_m(z-z_1) & p_m(z-z_2) & \ldots & p_m(z-z_n) \end{bmatrix}, \tag{16}$$

$$\boldsymbol{b}^{\mathrm{T}}(z) = (b_0(z), b_1(z), \ldots, b_m(z)). \tag{17}$$

2.3. Complex variable reproducing conditions

Here the correction coefficients are obtained via the following linear algebraic system of equations satisfying the reproducing conditions. In the CVRKPM, a Taylor series expansion of function $\bar{u}(z_I)$ is used and written as follows:

$$\bar{u}(z_I) = \bar{u}(z) + \sum_{k=1}^{\infty} \frac{(-1)^k}{k!}(z-z_I)^k \bar{u}^{(k)}(z). \tag{18}$$

Substituting Eq. (18) into Eq. (6) yields

$$\bar{u}^h(z) = \bar{m}_0(z)\bar{u}(z) + \sum_{k=1}^{\infty} \frac{(-1)^k}{k!}\bar{m}_k(z)\bar{u}^{(k)}(z), \tag{19}$$

where $\bar{m}_k(z)$ is the moment of the corrected weight function,

$$\begin{aligned}\bar{m}_k(z) &= \sum_{I}^{n} (z-z_I)^k \bar{w}_{\mathrm{h}}(z-z_I)\Delta V_I, \\ &\quad (k=0,1,2,\ldots).\end{aligned} \tag{20}$$

For the kernel estimate to reproduce a unity, the moment of kernel function is enforced to satisfy the

following conditions, i.e., zero-th order reproducing conditions:

$$\bar{m}_0(z) = 1. \tag{21}$$

In order to reproduce a linear function $\bar{u}(z) = a_0 + a_1 z$, the following reproducing conditions

$$\bar{m}_0(z) = 1, \quad \bar{m}_1(z) = 0 \tag{22}$$

must be satisfied. And, to reproduce an m-th order polynomial, the reproducing conditions can be written as

$$\bar{m}_0(z) = 1, \quad \bar{m}_1(z) = 0, \ldots, \bar{m}_m(z) = 0. \tag{23}$$

Substituting Eqs. (2) and (3) into Eq. (20), and considering the reproducing conditions Eq. (23), we have

$$\boldsymbol{M}(z)\boldsymbol{b}(z) = \begin{pmatrix} \bar{m}_0(z) \\ \bar{m}_1(z) \\ \vdots \\ \bar{m}_m(z) \end{pmatrix} = \begin{pmatrix} 1 \\ 0 \\ \vdots \\ 0 \end{pmatrix}, \tag{24}$$

where

$$\begin{aligned} \boldsymbol{M}(z) &= \begin{bmatrix} m_0(z) & m_1(z) & \ldots & m_m(z) \\ m_1(z) & m_2(z) & \ldots & m_{m+1}(z) \\ \vdots & \vdots & \ddots & \vdots \\ m_m(z) & m_{m+1}(z) & \ldots & m_{2m}(z) \end{bmatrix} \\ &= \sum_{I=1}^{n} \boldsymbol{p}(z - z_I) \cdot \boldsymbol{p}^{\mathrm{T}}(z - z_I) \\ &\quad \cdot w_{\mathrm{h}}(z - z_I) \cdot \Delta V_I. \end{aligned} \tag{25}$$

Let

$$\boldsymbol{H} = (1, 0, \ldots, 0)^{\mathrm{T}}, \tag{26}$$

Equation (24) can be written in matrix form as

$$\boldsymbol{M}(z) \cdot \boldsymbol{b}(z) = \boldsymbol{H}; \tag{27}$$

and then we have

$$\boldsymbol{b}(z) = \boldsymbol{M}^{-1}(z) \cdot \boldsymbol{H}. \tag{28}$$

2.4. The shape function of the CVRKPM

From Eq. (8), the expression of the trial function $\bar{u}^h(z)$ can be written as

$$\bar{u}^h(z) = \boldsymbol{\Phi}(z)\bar{\boldsymbol{u}} = \sum_{I=1}^{n} \Phi_I(z)\bar{u}(z_I), \tag{29}$$

and then we have

$$u_1^h(z) = \mathrm{Re}[\boldsymbol{\Phi}(z)\bar{\boldsymbol{u}}] = \mathrm{Re}\left[\sum_{I=1}^{n} \Phi_I(z)\bar{u}(z_I)\right], \tag{30}$$

$$u_2^h(z) = \mathrm{Im}[\boldsymbol{\Phi}(z)\bar{\boldsymbol{u}}] = \mathrm{Im}\left[\sum_{I=1}^{n} \Phi_I(z)\bar{u}(z_I)\right], \tag{31}$$

where $\boldsymbol{\Phi}(z)$ is the shape function of the CVRKPM, and

$$\begin{aligned} \boldsymbol{\Phi}(z) &= (\Phi_1(z), \Phi_2(z), \ldots, \Phi_n(z)) \\ &= \boldsymbol{C}(z)\boldsymbol{W}(z)\boldsymbol{V}, \end{aligned} \tag{32}$$

$$\Phi_I(z) = C(z; z - z_I) w_{\mathrm{h}}(z - z_I) \Delta V_I. \tag{33}$$

The advantages of the CVRKPM are that the correction function of a 2D problem is formed with 1D basis function, which leads to the fewer nodes that can be selected in the domain of a problem when the meshless method formed with the CVRKPM is used, because the unknown coefficients in the CVRKPM are fewer than in the RKPM. For the linear basis, the basis function in the RKPM is $\boldsymbol{p}^{\mathrm{T}} = (1, x_1 - x_1', x_2 - x_2')$, and three unknown coefficients are needed; and the basis function in the CVRKPM is $\boldsymbol{p}^{\mathrm{T}} = (1, z - z')$, and two unknown coefficients are needed. For the quadratic basis, if the basis function in the RKPM is $\boldsymbol{p}^{\mathrm{T}} = (1,\ x_1 - x_1', x_2 - x_2', (x_1 - x_1')^2, (x_1 - x_1')(x_2 - x_2'), (x_2 - x_2')^2)$, then six unknown coefficients are needed; however, the basis function in the CVRKPM is $\boldsymbol{p}^{\mathrm{T}} = \left(1, z - z', (z - z')^2\right)$, and thus three unknown coefficients are needed. Then for an arbitrary point in the domain, we need fewer nodes with support domains that cover the point, and so we also require fewer nodes in the entire domain of a problem. Under the same node distribution in the problem domain, the CVRKPM has greater precision than the RKPM.

In addition, for an arbitrary node, when its shape function and the derivatives of this function are formed, it is necessary to obtain the inversion of the matrix $\boldsymbol{M}$ and the product of matrices. Under the same precision, because fewer unknown coefficients are needed in the CVRKPM, thus reducing the dimension of the matrix $\boldsymbol{M}$, we can obtain the inversion of the matrix $\boldsymbol{M}$ and the product of matrices simply and rapidly, and then the CVRKPM has greater computational efficiency than the RKPM.

3. The CVRKPM for 2D linear elastodynamics

This section presents a detailed procedure of the CVRKPM for the 2D linear elastodynamics.

The governing equations, boundary condition and the initial condition of the 2D linear elastodynamics can be written as follows:

$$\boldsymbol{L}^{\mathrm{T}}\boldsymbol{\sigma}+\boldsymbol{b}=\rho\ddot{\boldsymbol{u}}+\mu\dot{\boldsymbol{u}}, \quad (\text{in} \quad \Omega); \tag{34}$$

$$\boldsymbol{u}=\bar{\boldsymbol{u}}, \quad (\text{on} \quad \Gamma_u); \tag{35}$$

$$\boldsymbol{n}\cdot\boldsymbol{\sigma}=\bar{\boldsymbol{t}}, \quad (\text{on} \quad \Gamma_t); \tag{36}$$

$$\boldsymbol{u}(z,t_0)=\boldsymbol{u}_0(z), \quad (\text{in} \quad \Omega); \tag{37a}$$

$$\dot{\boldsymbol{u}}(z,t_0)=\boldsymbol{v}_0(z), \quad (\text{in} \quad \Omega); \tag{37b}$$

where $\boldsymbol{L}$ is differential operator matrix, i.e.

$$\boldsymbol{L}=\begin{bmatrix} \dfrac{\partial}{\partial x_1} & 0 \\ 0 & \dfrac{\partial}{\partial x_2} \\ \dfrac{\partial}{\partial x_2} & \dfrac{\partial}{\partial x_1} \end{bmatrix}, \tag{38}$$

$\boldsymbol{\sigma}$ is the stress vector,

$$\boldsymbol{\sigma}=\begin{bmatrix} \sigma_{11} \\ \sigma_{22} \\ \sigma_{12} \end{bmatrix}, \tag{39}$$

$\boldsymbol{b}$ is the external body force vector,

$$\boldsymbol{b}=\begin{bmatrix} b_1(t) \\ b_2(t) \end{bmatrix}, \tag{40}$$

ρ is the mass density, μ is damping coefficient, $\boldsymbol{u}$, $\dot{\boldsymbol{u}}$, and $\ddot{\boldsymbol{u}}$ are the vectors of the displacement, velocity, and acceleration, respectively,

$$\boldsymbol{u}=\begin{bmatrix} u_1(t) \\ u_2(t) \end{bmatrix}, \tag{41}$$

$$\dot{\boldsymbol{u}}=\begin{bmatrix} \dot{u}_1(t) \\ \dot{u}_2(t) \end{bmatrix}, \tag{42}$$

$$\ddot{\boldsymbol{u}}=\begin{bmatrix} \ddot{u}_1(t) \\ \ddot{u}_2(t) \end{bmatrix}. \tag{43}$$

Here $\bar{\boldsymbol{u}}$ is the prescribed displacement on the essential boundary Γ_u, $\bar{\boldsymbol{t}}$ is the prescribed traction on the natural boundary Γ_t, $\boldsymbol{n}$ is the component of the unit normal to the natural boundary Γ_t, and $\boldsymbol{u}_0$ and $\boldsymbol{v}_0$ is the initial displacement and velocity at an arbitrary point z, respectively. Γ is the boundary of the domain Ω, and $\Gamma=\Gamma_u\cup\Gamma_t$, $\Gamma_u\cap\Gamma_t=\emptyset$.

The stress–strain relationship can be expressed as

$$\boldsymbol{\sigma}=\boldsymbol{D}\boldsymbol{\varepsilon}, \tag{44}$$

where $\boldsymbol{D}$ is material constant matrix. For isotropic materials, we have

$$\boldsymbol{D}=\frac{E}{1-\nu^2}\begin{bmatrix} 1 & \nu & 0 \\ \nu & 1 & 0 \\ 0 & 0 & \dfrac{1-\nu}{2} \end{bmatrix} \tag{45}$$

for plane stress problems; and

$$\boldsymbol{D}=\frac{E}{(1+\nu)(1-2\nu)}\begin{bmatrix} 1-\nu & \nu & 0 \\ \nu & 1-\nu & 0 \\ 0 & 0 & \dfrac{1-2\nu}{2} \end{bmatrix} \tag{46}$$

for plane strain problems. Here E is Young's modulus, and ν is Poisson's ratio.

The strain–displacement relationship can be written as

$$\boldsymbol{\varepsilon}=\boldsymbol{L}\boldsymbol{u}, \tag{47}$$

here the Galerkin weak form is employed to develop the discretised system equation. Because the shape functions of the CVRKPM do not satisfy the property of the Kronecker δ function, the essential boundary conditions cannot be applied directly. The Penalty method, which is one of the most widely used techniques to enforce the essential boundary conditions, is used in this paper. And the corresponding constrained Galerkin weak form can be given by

$$\begin{aligned} &\int_\Omega \delta\boldsymbol{u}^{\mathrm{T}}\rho\ddot{\boldsymbol{u}}\mathrm{d}\Omega+\int_\Omega \delta\boldsymbol{u}^{\mathrm{T}}\mu\dot{\boldsymbol{u}}\mathrm{d}\Omega \\ &+\int_\Omega \delta\boldsymbol{\varepsilon}^{\mathrm{T}}\boldsymbol{\sigma}\mathrm{d}\Omega-\int_\Omega \delta\boldsymbol{u}^{\mathrm{T}}\boldsymbol{b}\mathrm{d}\Omega-\int_{\Gamma_t}\delta\boldsymbol{u}^{\mathrm{T}}\bar{\boldsymbol{t}}\mathrm{d}\Gamma \\ &+\alpha\int_{\Gamma_u}\delta\boldsymbol{u}^{\mathrm{T}}\boldsymbol{S}(\boldsymbol{u}-\bar{\boldsymbol{u}})\mathrm{d}\Gamma=0, \end{aligned} \tag{48}$$

where

$$\boldsymbol{S}=\begin{bmatrix} s_1 & 0 \\ 0 & s_2 \end{bmatrix}, \tag{49}$$

$$s_i = \begin{cases} 1, \text{ if } u_i \text{ is the prescribed displacement on } \Gamma_u, \\ 0, \text{ if } u_i \text{ is not the prescribed displacement on } \Gamma_u, \end{cases} \tag{50}$$

and α is penalty factor which is a function of coordinates. To apply the boundary conditions completely, the penalty factor must be infinite, which is not possible in practical numerical analysis. In general, a large positive number of penalty factor is used to enforce the boundary conditions. In this paper, when

$$\alpha = (1 \times 10^5 E \sim 1 \times 10^8 E), \tag{51}$$

the solution will have good precision.

By using the stress–strain relationship Eq. (44) and the strain–displacement relationship Eq. (47), Eq. (48) can be explicitly expressed as

$$\begin{aligned} &\int_\Omega \delta \boldsymbol{u}^{\mathrm{T}} \rho \ddot{\boldsymbol{u}} \mathrm{d}\Omega + \int_\Omega \delta \boldsymbol{u}^{\mathrm{T}} \mu \dot{\boldsymbol{u}} \mathrm{d}\Omega \\ &+ \int_\Omega \delta (\boldsymbol{L}\boldsymbol{u})^{\mathrm{T}} \boldsymbol{D} (\boldsymbol{L}\boldsymbol{u}) \mathrm{d}\Omega - \int_\Omega \delta \boldsymbol{u}^{\mathrm{T}} \boldsymbol{b} \mathrm{d}\Omega \\ &- \int_{\Gamma_t} \delta \boldsymbol{u}^{\mathrm{T}} \bar{\boldsymbol{t}} \mathrm{d}\Gamma + \alpha \int_{\Gamma_u} \delta \boldsymbol{u}^{\mathrm{T}} \boldsymbol{S} (\boldsymbol{u} - \bar{\boldsymbol{u}}) \mathrm{d}\Gamma = 0. \end{aligned} \tag{52}$$

For 2D linear elastodynamic problems, displacement trial function at any point z is a function of spatial coordinate z and time t. In this paper, we only need to discretise the space domain at an arbitrary time t.

Because the shape functions are time independent, the node displacements are functions of time only, and then from the approximation function (29), the displacements $u_1(z,t)$ and $u_2(z,t)$ at an arbitrary point $z = x_1 + ix_2$ in the domain can be expressed as

$$\bar{u}^h(z,t) = u_1^h(z,t) + \mathrm{i}\, u_2^h(z,t) = \sum_{I=1}^{n} \Phi_I(z) \bar{u}_I(t), \tag{53}$$

where the parameter $\bar{u}_I(t)$ associated with node z_I can be written as

$$\bar{u}_I(t) = u_1(z_I,t) + \mathrm{i}\, u_2(z_I,t). \tag{54}$$

From Eqs. (53) and (54), we have

$$\boldsymbol{u}^h(t) = \begin{pmatrix} u_1^h(z,t) \\ u_2^h(z,t) \end{pmatrix} = \sum_I^n \begin{bmatrix} \mathrm{Re}[\Phi_I(z)] & -\mathrm{Im}[\Phi_I(z)] \\ \mathrm{Im}[\Phi_I(z)] & \mathrm{Re}[\Phi_I(z)] \end{bmatrix} \cdot \begin{pmatrix} u_1(z_I,t) \\ u_2(z_I,t) \end{pmatrix} = \sum_I^n \tilde{\boldsymbol{\Phi}}_I(z) \cdot \boldsymbol{u}_I(t), \tag{55}$$

where $\tilde{\boldsymbol{\Phi}}_I$ is the matrix of shape functions, and

$$\tilde{\boldsymbol{\Phi}}_I(z) = \begin{bmatrix} \mathrm{Re}[\Phi_I(z)] & -\mathrm{Im}[\Phi_I(z)] \\ \mathrm{Im}[\Phi_I(z)] & \mathrm{Re}[\Phi_I(z)] \end{bmatrix}, \tag{56}$$

$\boldsymbol{u}_I(t)$ is node displacement parameter vector at node z_I, i.e.

$$\boldsymbol{u}_I(t) = (u_1(z_I,t), u_2(z_I,t))^{\mathrm{T}}, \quad I = 1, 2, \ldots, n. \tag{57}$$

Similarly, we can obtain the formulae of the acceleration and velocity at the point z as follows:

$$\ddot{\boldsymbol{u}}^h(t) = \begin{pmatrix} \ddot{u}_1^h(z,t) \\ \ddot{u}_2^h(z,t) \end{pmatrix} = \sum_I^n \begin{bmatrix} \mathrm{Re}[\Phi_I(z)] & -\mathrm{Im}[\Phi_I(z)] \\ \mathrm{Im}[\Phi_I(z)] & \mathrm{Re}[\Phi_I(z)] \end{bmatrix} \cdot \begin{pmatrix} \ddot{u}_1(z_I,t) \\ \ddot{u}_2(z_I,t) \end{pmatrix} = \sum_I^n \tilde{\boldsymbol{\Phi}}_I(z) \cdot \ddot{\boldsymbol{u}}_I(t), \tag{58}$$

$$\dot{\boldsymbol{u}}^h(t) = \begin{pmatrix} \dot{u}_1^h(z,t) \\ \dot{u}_2^h(z,t) \end{pmatrix} = \sum_I^n \begin{bmatrix} \mathrm{Re}[\Phi_I(z)] & -\mathrm{Im}[\Phi_I(z)] \\ \mathrm{Im}[\Phi_I(z)] & \mathrm{Re}[\Phi_I(z)] \end{bmatrix} \cdot \begin{pmatrix} \dot{u}_1(z_I,t) \\ \dot{u}_2(z_I,t) \end{pmatrix} = \sum_I^n \tilde{\boldsymbol{\Phi}}_I(z) \cdot \dot{\boldsymbol{u}}_I(t), \tag{59}$$

where $\ddot{\boldsymbol{u}}_I$ and $\dot{\boldsymbol{u}}_I(t)$ are node acceleration and velocity vectors at node z_I, respectively,

$$\ddot{\boldsymbol{u}}_I(t) = (\ddot{u}_1(z_I,t), \ddot{u}_2(z_I,t))^{\mathrm{T}}, \quad I = 1, 2, \ldots, n; \tag{60}$$

$$\dot{\boldsymbol{u}}_I(t) = (\dot{u}_1(z_I,t), \dot{u}_2(z_I,t))^{\mathrm{T}}, \quad I = 1, 2, \ldots, n. \tag{61}$$

From Eq. (55), we have

$$\boldsymbol{L}\boldsymbol{u}^h = \boldsymbol{L}\sum_I^n \tilde{\boldsymbol{\Phi}}_I \boldsymbol{u}_I(t) = \sum_I^n \boldsymbol{L}\tilde{\boldsymbol{\Phi}}_I \boldsymbol{u}_I(t) = \sum_I^n \begin{bmatrix} \dfrac{\partial}{\partial x_1} & 0 \\ 0 & \dfrac{\partial}{\partial x_2} \\ \dfrac{\partial}{\partial x_2} & \dfrac{\partial}{\partial x_1} \end{bmatrix} \begin{bmatrix} \mathrm{Re}[\Phi_I] & -\mathrm{Im}[\Phi_I] \\ \mathrm{Im}[\Phi_I] & \mathrm{Re}[\Phi_I] \end{bmatrix} \cdot \boldsymbol{u}_I(t)$$

$$= \sum_I^n \begin{bmatrix} \mathrm{Re}[\Phi_{I,1}] & -\mathrm{Im}[\Phi_{I,1}] \\ \mathrm{Im}[\Phi_{I,2}] & \mathrm{Re}[\Phi_{I,2}] \\ \mathrm{Re}[\Phi_{I,2}] + \mathrm{Im}[\Phi_{I,1}] & \mathrm{Re}[\Phi_{I,1}] - \mathrm{Im}[\Phi_{I,2}] \end{bmatrix} \cdot \boldsymbol{u}_I(t) = \sum_I^n \boldsymbol{B}_I \boldsymbol{u}_I(t), \tag{62}$$

where $\Phi_{I,i}$ represent the derivatives of the complex variable reproducing kernel particle shape function with respect to x_i, and $\boldsymbol{B}_I$ is the strain matrix for node z_I,

$$\boldsymbol{B}_I = \begin{bmatrix} \mathrm{Re}[\Phi_{I,1}] & -\mathrm{Im}[\Phi_{I,1}] \\ \mathrm{Im}[\Phi_{I,2}] & \mathrm{Re}[\Phi_{I,2}] \\ \mathrm{Re}[\Phi_{I,2}] + \mathrm{Im}[\Phi_{I,1}] & \mathrm{Re}[\Phi_{I,1}] - \mathrm{Im}[\Phi_{I,2}] \end{bmatrix}. \tag{63}$$

Substituting Eqs. (55), (58), (59), and (62) into Eq. (52), we have

$$\int_\Omega \delta\Big(\sum_I^n \tilde{\boldsymbol{\Phi}}_I \boldsymbol{u}_I\Big)^{\mathrm{T}} \cdot \rho \cdot \Big(\sum_J^n \tilde{\boldsymbol{\Phi}}_I \ddot{\boldsymbol{u}}_J\Big)\mathrm{d}\Omega + \int_\Omega \delta\Big(\sum_I^n \tilde{\boldsymbol{\Phi}}_I \boldsymbol{u}_I\Big)^{\mathrm{T}} \cdot \mu \cdot \Big(\sum_J^n \tilde{\boldsymbol{\Phi}}_J \dot{\boldsymbol{u}}_J\Big)\mathrm{d}\Omega$$
$$+ \int_\Omega \delta\Big(\sum_I^n \boldsymbol{B}_I \boldsymbol{u}_I\Big)^{\mathrm{T}} D\Big(\sum_J^n \boldsymbol{B}_J \boldsymbol{u}_J\Big)\mathrm{d}\Omega - \int_\Omega \delta\Big(\sum_I^n \tilde{\boldsymbol{\Phi}}_I \boldsymbol{u}_I\Big)^{\mathrm{T}} \boldsymbol{b}\mathrm{d}\Omega - \int_{\Gamma_t} \delta\Big(\sum_I^n \tilde{\boldsymbol{\Phi}}_I \boldsymbol{u}_I\Big)^{\mathrm{T}} \bar{\boldsymbol{t}}\mathrm{d}\Gamma$$
$$+\alpha \int_{\Gamma_u} \delta\Big(\sum_I^n \tilde{\boldsymbol{\Phi}}_I \boldsymbol{u}_I\Big)^{\mathrm{T}} \boldsymbol{S}\Big(\sum_J^n \tilde{\boldsymbol{\Phi}}_J \boldsymbol{u}_J\Big)\mathrm{d}\Gamma + \alpha \int_{\Gamma_u} \delta\Big(\sum_I^n \tilde{\boldsymbol{\Phi}}_I \boldsymbol{u}_I\Big)^{\mathrm{T}} \boldsymbol{S} \cdot \bar{\boldsymbol{u}}\mathrm{d}\Gamma = 0. \tag{64}$$

Finally, we can obtain the equation of motion as follows:

$$\boldsymbol{M}\ddot{\boldsymbol{U}}(t) + \boldsymbol{C}\dot{\boldsymbol{U}}(t) + (\boldsymbol{K} + \boldsymbol{K}^\alpha)\boldsymbol{U}(t) = \boldsymbol{F}(t) + \boldsymbol{F}^\alpha, \tag{65}$$

where $\boldsymbol{K}$ is the global stiffness matrix, $\boldsymbol{M}$ is the global mass matrix, $\boldsymbol{C}$ is the damping matrix, $\boldsymbol{F}$ is the global external force vector, $\boldsymbol{K}^\alpha$ is the global penalty matrix, and the vector $\boldsymbol{F}^\alpha$ is also caused by the essential boundary condition. The elements of the matrices $\boldsymbol{M}$, $\boldsymbol{K}$, $\boldsymbol{C}$, $\boldsymbol{K}^\alpha$ and the vectors $\boldsymbol{F}$ and $\boldsymbol{F}^\alpha$ are given as

$$\boldsymbol{M}_{IJ} = \int_\Omega \tilde{\boldsymbol{\Phi}}_I^{\mathrm{T}} \cdot \rho \cdot \tilde{\boldsymbol{\Phi}}_J \mathrm{d}\Omega, \tag{66}$$

$$\boldsymbol{C}_{IJ} = \int_\Omega \tilde{\boldsymbol{\Phi}}_I^{\mathrm{T}} \cdot \mu \cdot \tilde{\boldsymbol{\Phi}}_J \mathrm{d}\Omega, \tag{67}$$

$$\boldsymbol{K}_{IJ} = \int_\Omega \boldsymbol{B}_I^{\mathrm{T}} \cdot \boldsymbol{D} \cdot \boldsymbol{B}_J \mathrm{d}\Omega, \tag{68}$$

$$\boldsymbol{K}_{IJ}^\alpha = \alpha \int_{\Gamma_u} \tilde{\boldsymbol{\Phi}}_I^{\mathrm{T}} \cdot \boldsymbol{S} \cdot \tilde{\boldsymbol{\Phi}}_J \mathrm{d}\Gamma, \tag{69}$$

$$\boldsymbol{f}_I(t) = \int_\Omega \tilde{\boldsymbol{\Phi}}_I^{\mathrm{T}} \boldsymbol{b}\mathrm{d}\Omega + \int_{\Gamma_t} \tilde{\boldsymbol{\Phi}}_I^{\mathrm{T}} \bar{\boldsymbol{t}}\mathrm{d}\Gamma, \tag{70}$$

$$\boldsymbol{f}_I^\alpha = \alpha \int_{\Gamma_u} \tilde{\boldsymbol{\Phi}}_I^{\mathrm{T}} \cdot \boldsymbol{S} \cdot \bar{\boldsymbol{u}}\mathrm{d}\Gamma. \tag{71}$$

In Eq. (65), $\ddot{\boldsymbol{U}}(t)$, $\dot{\boldsymbol{U}}(t)$ and $\boldsymbol{U}(t)$ are global acceleration, velocity and displacement vectors at all nodes in the entire problem domain, respectively,

$$\ddot{\boldsymbol{U}} = \big(\ddot{\boldsymbol{u}}_1^{\mathrm{T}}(t), \ddot{\boldsymbol{u}}_2^{\mathrm{T}}(t), \ldots, \ddot{\boldsymbol{u}}_n^{\mathrm{T}}(t)\big)^{\mathrm{T}}, \tag{72}$$

$$\dot{\boldsymbol{U}} = \big(\dot{\boldsymbol{u}}_1^{\mathrm{T}}(t), \dot{\boldsymbol{u}}_2^{\mathrm{T}}(t), \ldots, \dot{\boldsymbol{u}}_n^{\mathrm{T}}(t)\big)^{\mathrm{T}}, \tag{73}$$

$$\boldsymbol{U} = \big(\boldsymbol{u}_1^{\mathrm{T}}(t), \boldsymbol{u}_2^{\mathrm{T}}(t), \ldots, \boldsymbol{u}_n^{\mathrm{T}}(t)\big)^{\mathrm{T}}. \tag{74}$$

Let

$$\bar{\boldsymbol{K}} = \boldsymbol{K} + \boldsymbol{K}^\alpha, \tag{75}$$

$$\bar{\boldsymbol{F}}(t) = \boldsymbol{F}(t) + \boldsymbol{F}^\alpha(t). \tag{76}$$

Equation (65) can be simply written as

$$\boldsymbol{M}\ddot{\boldsymbol{U}}(t) + \boldsymbol{C}\dot{\boldsymbol{U}}(t) + \bar{\boldsymbol{K}}\boldsymbol{U}(t) = \bar{\boldsymbol{F}}(t). \tag{77}$$

If damping is not considered, Eq. (77) will be

$$\boldsymbol{M}\ddot{\boldsymbol{U}}(t) + \bar{\boldsymbol{K}}\boldsymbol{U}(t) = \bar{\boldsymbol{F}}(t). \tag{78}$$

4. Implicit time integration

The simulation of a complex elastodynamic problem requires a high efficient algorithm of time inte-

gration. Many approaches have been established to solve different linear elastodynamics problems. They are mainly classified into explicit and implicit algorithms. The advantage of an explicit approach is that it avoids solving algebraic equations at each time step, which leads to less computational cost. However, the inherent disadvantage of an explicit approach is that it is conditionally stable. In order to overcome this disadvantage, some implicit approaches are proposed to achieve unconditional stability for large time-step, e.g., Wilson-θ method, Newmark-β method and Runge–Kutta method. In this paper, the classical Newmark-β algorithm,[32,51,52] which has been the most popular algorithm to perform dynamic analysis, is adopted for the time discretisation of the equations of motion.

The time domain T will be discretised by n time increments, and $\Delta t(= T/n)$. We assume that the analysis starts at time t and the displacement $\boldsymbol{U}_t$ and its derivatives are known, then from $\boldsymbol{U}_t$, $\dot{\boldsymbol{U}}_t$, $\ddot{\boldsymbol{U}}_t$ we will obtain $\boldsymbol{U}_{t+\Delta t}$, $\dot{\boldsymbol{U}}_{t+\Delta t}$, $\ddot{\boldsymbol{U}}_{t+\Delta t}$. Applying the Taylor expansion of $\dot{\boldsymbol{U}}_{t+\Delta t}$ and $\boldsymbol{U}_{t+\Delta t}$ at the time step t, we have

$$\boldsymbol{U}_{t+\Delta t} = \boldsymbol{U}_t + \Delta t\dot{\boldsymbol{U}}_t + \frac{1}{2}(1-\beta_2)\Delta t^2\ddot{\boldsymbol{U}}_t + \frac{1}{2}\beta_2\Delta t^2\ddot{\boldsymbol{U}}_{t+\Delta t}, \tag{79}$$

$$\dot{\boldsymbol{U}}_{t+\Delta t} = \dot{\boldsymbol{U}}_t + (1-\beta_1)\Delta t\ddot{\boldsymbol{U}}_t + \beta_1\Delta t\ddot{\boldsymbol{U}}_{t+\Delta t}. \tag{80}$$

From Eq. (79), we have

$$\ddot{\boldsymbol{U}}_{t+\Delta t} = \frac{2}{\beta_2\Delta t^2}(\boldsymbol{U}_{t+\Delta t} - \boldsymbol{U}_t) - \frac{2}{\beta_2\Delta t}\dot{\boldsymbol{U}}_t - \left(\frac{1}{\beta_2} - 1\right)\ddot{\boldsymbol{U}}_t. \tag{81}$$

Let

$$\alpha_1 = \frac{2}{\beta_2\Delta t^2}, \tag{82}$$

$$\alpha_2 = \frac{2}{\beta_2\Delta t}, \tag{83}$$

$$\alpha_3 = \frac{1}{\beta_2} - 1, \tag{84}$$

Equation (81) can be written simply as

$$\ddot{\boldsymbol{U}}_{t+\Delta t} = \alpha_1(\boldsymbol{U}_{t+\Delta t} - \boldsymbol{U}_t) - \alpha_2\dot{\boldsymbol{U}}_t - \alpha_3\ddot{\boldsymbol{U}}_t. \tag{85}$$

Substituting Eq. (85) into Eq. (80) yields

$$\dot{\boldsymbol{U}}_{t+\Delta t} = \beta_1\alpha_2(\boldsymbol{U}_{t+\Delta t} - \boldsymbol{U}_t) + \left(1 - \frac{2\beta_1}{\beta_2}\right)\dot{\boldsymbol{U}}_t + \left(1 - \frac{\beta_1}{\beta_2}\right)\Delta t\ddot{\boldsymbol{U}}_t. \tag{86}$$

Equation (77) can be written as

$$\boldsymbol{M}\ddot{\boldsymbol{U}}_{t+\Delta t} + \boldsymbol{C}\dot{\boldsymbol{U}}_{t+\Delta t} + \bar{\boldsymbol{K}}\boldsymbol{U}_{t+\Delta t} = \bar{\boldsymbol{F}}_{t+\Delta t}. \tag{87}$$

Substituting Eqs. (85) and (86) into Eq. (87), we have

$$\left(\alpha_1\boldsymbol{M} + \beta_1\alpha_2\boldsymbol{C} + \bar{\boldsymbol{K}}\right)\boldsymbol{U}_{t+\Delta t} = \bar{\boldsymbol{F}}_{t+\Delta t} + \boldsymbol{M}\left(\alpha_1\boldsymbol{U}_t + \alpha_2\dot{\boldsymbol{U}}_t + \alpha_3\ddot{\boldsymbol{U}}_t\right) + \boldsymbol{C}\left[\beta_1\alpha_2\boldsymbol{U}_t + \left(\frac{2\beta_1}{\beta_2} - 1\right)\dot{\boldsymbol{U}}_t + \left(\frac{\beta_1}{\beta_2} - 1\right)\Delta t\ddot{\boldsymbol{U}}_t\right], \tag{88}$$

where β_1 and β_2 are the Newmark's parameters which are related to the stability and precision. Different choices of parameters β_1 and β_2 will lead to different Newmark method. The Newmark method is unconditionally stable if

$$\beta_1 \geq \frac{1}{2}, \quad \text{and} \quad \beta_2 \geq \frac{1}{2}\cdot\left(\frac{1}{2} + \beta_1\right). \tag{89}$$

In this paper, the parameters $\beta_1 = 3/2$ and $\beta_2 = 8/5$ is used, and the method is called Galerkin method.

Equations (80), (85), and (88) are the final recurrence equations for the Newmark-β method.

5. Numerical examples

In this section, some numerical examples of the CVRKPM in two-dimensional linear elastodynamic problems are presented to demonstrate the accuracy and advantage of the CVRKPM.

5.1. Cantilever beam problem

Consider a cantilever beam subjected to a Heaviside type load at the free end of $t = 0$ s which is kept constant in time (see Fig. 1). The material constants are the density $\rho = 10000$ kg/m^3, the Young's modulus $E = 210$ GPa, and the Poisson's ratio $\nu = 0.3$. The dynamic load is shown in Fig. 2, with $p = 1$ N/m^2. The length of the beam is $l = 100$ cm,

and the height of the beam is $h = 10$ cm, and the beam with unit thickness in the plane stress state is considered. The initial displacement and velocity are zero, i.e. $\boldsymbol{u}_0 = \dot{\boldsymbol{u}}_0 = 0$. The essential boundary conditions are $u_1(0,t) = u_2(0,t) = 0$.

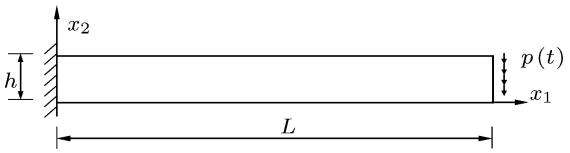


Fig. 1. Cantilever beam loaded with an external step force p.



Fig. 2. The dynamic load.

The analytical solution of the fundamental time period T of a cantilever beam can be obtained from the classical beam theory as

$$T = \frac{2\pi}{1.875^2}\sqrt{\frac{12\rho l^4}{Eh^2}}. \tag{90}$$

The maximum displacement w of the free end of the beam is estimated by calculating the bending deformation. The analytical solution of maximum displacement is obtained from the equation for static bending with a premultiplied factor of 2 for dynamic loading, and

$$w_{\max} = 2\frac{phl^3}{3EI}. \tag{91}$$

Using Eqs. (90) and (91), the analytical solution of vertical displacement at point A, which is the mid point of the free end of the beam, can be written as

$$w(t) = \frac{1}{2}\left[1 - \cos\left(\frac{2\pi}{T}t\right)\right]w_{\max}. \tag{92}$$

A regular distribution of 63 nodes is used in the domain, as shown in Fig. 3. The linear basis function is used to obtain the correction function. The time step chosen for the time integration is $\Delta t = 0.001$ s.

The analytical and the numerical solutions using the RKPM and CVRKPM are shown in Fig. 4. From which we can see that the results obtained with the CVRKPM agree well with the analytical solution and that the CVRKPM has greater precision than the conventional RKPM with the same node distribution.

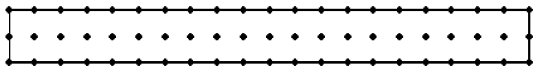


Fig. 3. Node distribution.

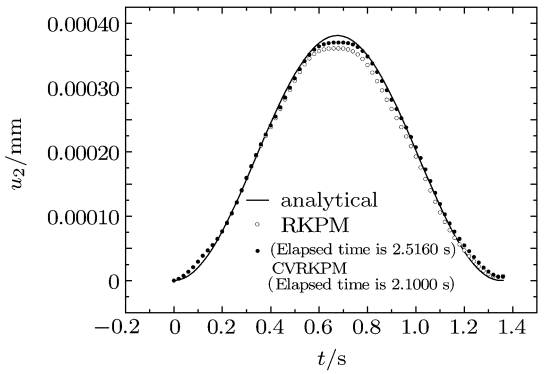


Fig. 4. Vertical displacement u_2 time-history at point A.

5.2. In-plane free vibration of a rectangular plate

The second example is an in-plane vibration problem of a rectangular plate, as shown in Fig. 5. The rectangular plate is fixed at all four sides, with distributed initial velocity. The initial conditions and boundary conditions are described as:

$$u_1(t) = u_2(t) = 0, \quad (\text{on } \Gamma_u), \tag{93}$$

$$u_1(x_1, x_2, t_0) = u_2(x_1, x_2, t_0) = 0, \quad (\text{in } \Omega), \tag{94}$$

$$\begin{aligned} \dot{u}_1(x_1, x_2, t_0) &= \dot{u}_2(x_1, x_2, t_0) \\ &= \frac{v_0 x_1(a - x_1)x_2(a - x_2)}{a^4}, \\ &\quad (\text{in } \Omega), \end{aligned} \tag{95}$$

where $v_0 = 100 \times 0.64^4$ m/s, both the initial deformation and initial force are zero.

This example is considered as a plane stress problem. The material properties are: density $\rho = 8.0 \times 10^5$ kg/m^3, Young's modulus $E = 100$ GPa, Poisson's ratio $\nu = 0.3$. And the width of the plate is $a = 320$ mm.

In Fig. 5, a regular distribution of 21×21 nodes is used. The time step is chosen as $\Delta t = 0.1 \times 10^{-3}$ ms. Because of the absence of an analytical solution, the

comparison between the CVRKPM and FEM numerical solutions are given in Figs. 6 and 7. Figure 6 shows the time history of displacement at the centre point in x_2 direction, while Fig. 7 shows the time history of velocity at the centre point in x_2 direction from 0 to 5 ms.

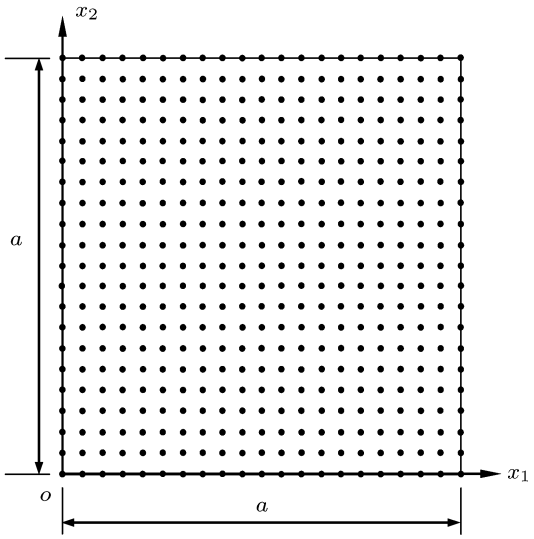


Fig. 5. Node distribution.

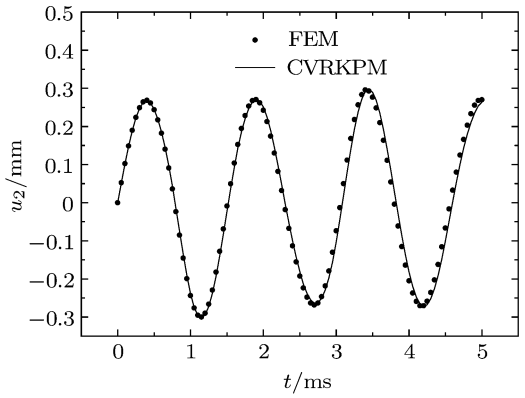


Fig. 6. The displacement u_2 at centre node.

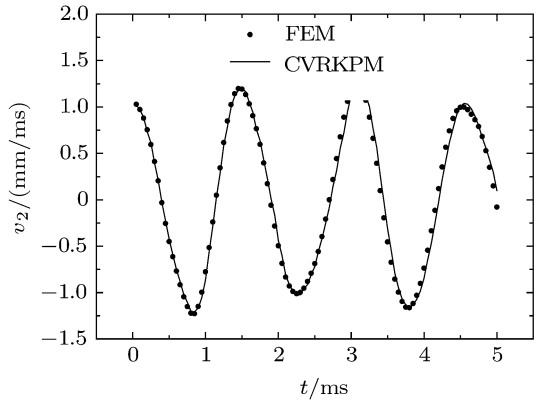


Fig. 7. The velocity v_2 at centre node.

From Figs. 6 and 7, we can conclude that numerical results obtained using the CVRKPM are in excellent agreement with those obtained using the FEM.

5.3. Beam-type medium for transient dynamic analysis

The third example is a beam-type medium with a cross section of 0.4 m×0.05 m subjected to a linearly distributed sudden normal pressure, as shown in Fig. 8. The dynamic load is shown in Fig. 2, with $p = 1$ GPa. The essential boundary conditions are $u_1(0,t) = u_2(0,t) = 0$.

The linearly elastic material constants are: density $\rho = 7850$ kg/m^3, Young's modulus $E = 200$ GPa, and the Poisson's ratio $\nu = 0.3$.

In Fig. 9, a regular node distribution of 41×6 nodes is used in the CVRKPM analysis. The time step is $\Delta t = 0.1 \times 10^{-6}$ s.

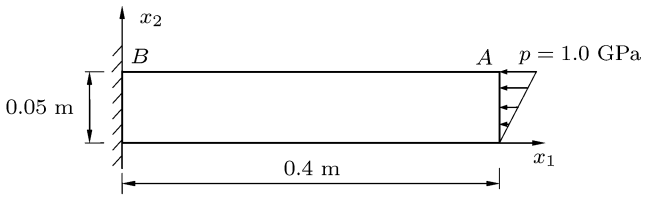


Fig. 8. Cantilever beam subjected to a linear pressure on the free edge.

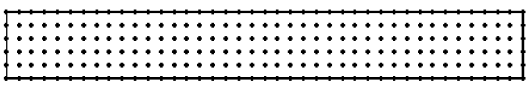


Fig. 9. Node distribution.

Because of the absence of an analytical solution, and in order to verify the correctness and effectiveness of the CVRKPM, the FEM is applied to solve the same problem. In the FEM analysis, two kinds of mesh of 246 nodes and 451 nodes are used. Results obtained by CVRKPM and the FEM are shown in Figs. 10–15. Figures 10 and 11 present the time histories of the displacements u_1 at point A. Figures 12 and 13 present the time histories of the displacements u_2 at the point A. The time histories of the total axial stress σ_{11} at point B are shown in Figs. 14 and 15. From Figs.10–15, compared with the FEM, the CVRKPM for 2D elastodynamics is proved to be efficient, and it has greater precision.

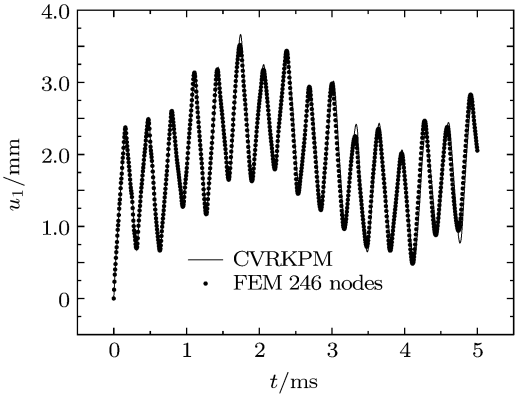


Fig. 10. Time history of the displacement u_1 at the top point A.

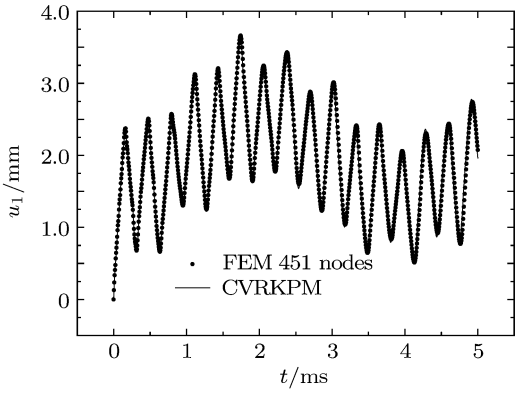


Fig. 11. Time history of the displacement u_1 at the top point A.

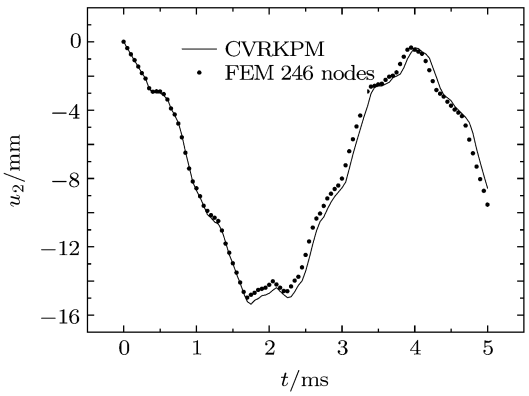


Fig. 12. Time history of the displacement u_2 at the top point A.

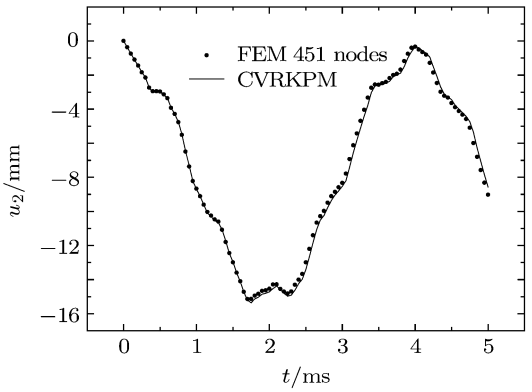


Fig. 13. Time history of the displacement u_2 at the top point A.

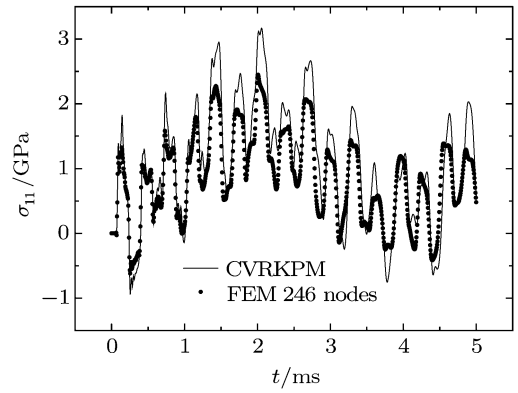


Fig. 14. Time history of the normal stress σ_{11} at the point B.

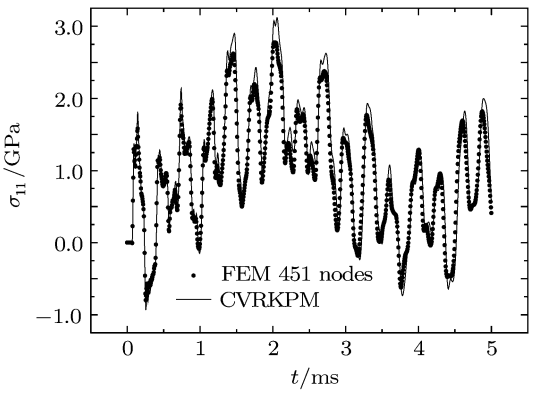


Fig. 15. Time history of the normal stress σ_{11} at the point B.

6. Conclusions

The complex variable reproducing kernel particle method (CVRKPM) has been discussed in this paper. The advantages of the complex variable reproducing kernel particle method are that the correction function of a 2D problem is formed with 1D basis function when the shape function is formed. Then the unknown coefficients of correction function in the complex variable reproducing kernel particle approximation are fewer than in the reproducing kernel particle approximation, then for an arbitrary point in the domain, we need fewer nodes with support domains that cover the point, and thus we also require fewer nodes

in the whole domain.

Three applications of the CVRKPM to 2D linear elastodynamics have been studied. The implicit meshless procedure was formed with discretisation by meshless in space and the Newmark algorithm in time. Compared with analytical solution, the present method is proved to be efficient. And it has greater precision than the conventional RKPM and FEM under the same number of nodes. It can be concluded that the CVRKPM is an effective numerical method for 2D elastodynamics.

References

[1] Yang Z J and Deeks A J 2007 *Comput. Mech.* **40** 725
[2] Belytschko T, Krongauz Y, Organ D, Fleming M and Krysl P 1996 *Comput. Meth. Appl. Mech. Eng.* **139** 3
[3] Li S F and Liu W K 2002 *Appl. Mech. Rev.* **55** 1
[4] Gingold R A and Monaghan J J 1977 *Mon. Not. R. Astron. Soc.* **18** 375
[5] Nayroles B, Touzot G and Villon P G 1992 *Comput. Mech.* **10** 307
[6] Belytschko T, Lu Y Y and Gu L 1994 *Int. J. Numer. Meth. Eng.* **37** 229
[7] Liu W K, Jun S and Zhang Y F 1995 *Int. J. Numer. Meth. Eng.* **20** 1081
[8] Onate E 1996 *Int. J. Numer. Meth. Eng.* **39** 3839
[9] Atluri S N and Zhu T L 1998 *Comput. Mech.* **22** 117
[10] Aluru N R 2000 *Int. J. Numer. Meth. Eng.* **47** 1083
[11] Liu W K and Chen Y J 1995 *Int. J. Numer. Meth. Fluids* **21** 901
[12] Wendland H 1999 *Math. Comput.* **68** 1521
[13] Idelsohn S R, Onate E and Calvo N 2003 *Int. J. Numer. Meth. Eng.* **58** 893
[14] Cheng Y M and Li J H 2005 *Acta Phys. Sin.* **54** 4463 (in Chinese)
[15] Cheng Y M and Li J H 2006 *Sci. China Ser. G Phys. Mech. Astron.* **49** 46
[16] Liew K M, Feng C, Cheng Y M and Kitipornchai S 2007 *Int. J. Numer. Meth. Eng.* **70** 46
[17] Chati M K, Mukherjee S and Mukherjee Y X 1999 *Int. J. Numer. Meth. Eng.* **46** 1163
[18] Zhu T, Zhang J and Atluri S N 1999 *Eng. Anal. Bound. Elem.* **23** 375
[19] Gu Y T and Liu G R 2003 *Struct. Eng. Mech.* **15** 535
[20] Liew K M, Cheng Y M and Kitipornchai S 2006 *Int. J. Numer. Meth. Eng.* **65** 1310
[21] Kitipornchai S, Liew K M and Cheng Y M 2005 *Comput. Mech.* **36** 13
[22] Cheng Y M and Peng M J 2005 *Sci. China Ser. G Phys. Mech. Astron.* **48** 641
[23] Liew K M, Cheng Y M and Kitipornchai S 2005 *Int. J. Numer. Meth. Eng.* **64** 1610
[24] Liew K M, Cheng Y M and Kitipornchai S 2007 *Int. J. Solids Struct.* **44** 4220
[25] Peng M J and Cheng Y M 2009 *Eng. Anal. Bound. Elem.* **33** 77
[26] Cheng Y M, Liew K M and Kitipornchai S 2009 *Int. J. Numer. Meth. Eng.* **78** 1258
[27] Ren H P and Zhang W 2009 *Chin. Phys.* B **18** 4065
[28] Lu Y Y, Belytschko T and Tabbara M 1995 *Comput. Meth. Appl. Mech. Eng.* **126** 131
[29] Liu W K, Jun S, Li S, Adee J and Belytschko T 1995 *Int. J. Numer. Meth. Eng.* **38** 1655
[30] Han Z D and Atluri S N 2004 *Comput. Mater. Continua* **1** 129
[31] Liu K Y, Long S Y and Li G Y 2006 *Eng. Anal. Bound. Elem.* **30** 72
[32] Gu Y T and Liu G R 2001 *Comput. Mech.* **27** 188
[33] Bueche D, Sukumar N and Moran B 2000 *Comput. Mech.* **25** 207
[34] Li S C, Li S C and Zhu W S 2006 *Chinese J. R. Mech. Eng.* **25** 141 (in Chinese)
[35] Li S C, Cheng Y M and Li S C 2006 *Acta Phys. Sin.* **55** 4760 (in Chinese)
[36] Sladek J, Sladek V and Keer R V 2003 *Int. J. Numer. Meth. Eng.* **57** 235
[37] Sellountos E J and Polyzos D 2005 *Comput. Mech.* **35** 265
[38] Li H, Wang Q X and Lam K Y 2004 *Comput. Meth. Appl. Mech. Eng.* **193** 2599
[39] Liew K M and Cheng Y M 2009 *Comput. Meth. Appl. Mech. Eng.* **198** 3925
[40] Monaghan J J 1988 *Comput. Phys. Commun.* **48** 89
[41] Liu W K, Chen Y, Jun S, Chen J S and Belytschko T 1996 *Arch. Comput. Meth. Eng.* **3** 3
[42] Zhou J X, Zhang H Y and Zhang L 2005 *J. Sound Vib.* **279** 389
[43] Zhang J P, Gong S G and Huang Y Q 2008 *Struct. Multidiscip. Optim.* **36** 307
[44] Kiani K, Nikkhoo A and Mehri B 2009 *J. Sound Vib.* **320** 632
[45] Gan N F, Li G Y and Long S Y 2009 *Eng. Anal. Bound. Elem.* **33** 1211
[46] Chen J S, Chen C, Wu C T and Liu W K 1996 *Comput. Meth. Appl. Mech. Eng.* **139** 195
[47] Liu W K and Jun S 1998 *Int. J. Numer. Meth. Eng.* **41** 1339
[48] Liu W K, Jun S, Thomas S D, Chen Y and Hao W 1997 *Int. J. Numer. Meth. Fluids* **24** 1391
[49] Chen L and Cheng Y M 2008 *Acta Phys. Sin.* **57** 1 (in Chinese)
[50] Chen L and Cheng Y M 2008 *Acta Phys. Sin.* **57** 6047 (in Chinese)
[51] Danielson K T, Hao S, Liu W K, Uras R A and Li S F 2000 *Int. J. Numer. Meth. Eng.* **47** 1323
[52] Ching H K 2002 *Solution of Linear Elastostatic and Elastodynamic Plane Problems by the Meshless Local Petrov–Galerkin Method* (Ph.D. Thesis) (Blacksburg: Virginia Polytechnic Institute and State University)